Published in final edited form as:
*NMR Biomed*. 2015 January ; 28(1): 63–69. doi:10.1002/nbm.3195.

# Measuring Renal Tissue Relaxation Times at 7T

**Xiufeng Li**[a,*], **Patrick J. Bolan**[a], **Kamil Ugurbil**[a], and **Gregory J. Metzger**[a]

[a]Center for Magnetic Resonance Research, University of Minnesota, Minneapolis, MN, United States

## Abstract

As developments in RF coils and RF management strategies make performing ultrahigh field renal imaging feasible, understanding the relaxation times of the tissue becomes increasingly important for tissue characterization and sequence optimization. By using a magnetization prepared single breath-hold fast spin echo imaging method, human renal $T_1$ and $T_2$ imaging studies were successfully performed at 7T while addressing challenges of B1+ inhomogeneity and peak short-term specific absorption rate (SAR). At 7T, measured renal $T_1$ values for the renal cortex and medulla (mean ± S.D.) were 1661 ± 68 ms and 2094 ± 67 ms, and $T_2$ values were 108 ± 7 ms and 126 ± 6 ms. For comparison, similar measurements were made at 3T where renal cortex and medulla $T_1$ values of 1261 ± 86 ms and 1676 ± 94 ms, and $T_2$ values of 121 ± 5 ms and 138 ± 7 ms were obtained. Measurements at 3T and 7T were significantly different for both $T_1$ and $T_2$ values in both renal tissues. Reproducibility studies at 7T demonstrated that $T_1$ and $T_2$ estimations were robust with group mean percentage differences of less than 4%.

### Keywords

longitudinal relaxation time (T1); transverse relaxation time (T2); renal relaxation time; kidneys; ultra high field; 7T

## INTRODUCTION

Motivated by the promise of higher signal noise ratio (SNR), increased resolution and/or reduced imaging time, new or better tissue contrast and improved parallel imaging performance, human MRI at ultrahigh magnetic fields (≥ 7T) has been a major research focus (1–5) despite the numerous challenges (6). Recently, with advances in RF coil engineering, RF shimming strategies and acquisition methods (7–10), UHF MRI technical development and translational research has been expanded from the human brain (5,11–14) to the abdominal and pelvic organs, e.g. heart, prostate and kidneys (15–26).

With respect to the kidney, increased SNR and reduced imaging time has the potential to reduce motion-related artifacts and improve imaging quality. For techniques such as arterial spin labeling (ASL) perfusion imaging, increased longitudinal relaxation times ($T_1$) and

*Correspondence to: Xiufeng Li, Ph.D., Center for Magnetic Resonance Research, University of Minnesota - Twin Cities, 2021 6th St. SE, Minneapolis, MN 55455, Tel: 612-625-7872, Fax: 612-626-2004, lixx1607@umn.edu.

SNR at 7T are particularly advantageous by enabling shorter acquisition times with the potential of high resolution, large organ coverage and in a single breath-hold (24–26).

Efficient, optimal and quantitative renal imaging requires the knowledge of tissue longitudinal ($T_1$) and transverse ($T_2$) relaxation times (27). Measuring renal $T_1$ and $T_2$ itself can also provide potentially valuable information for diagnosis and prognosis (28). For example, the potential of renal tissue $T_1$ to characterize and differentiate specific renal diseases states has been demonstrated (29–31). Renal tissue $T_1$ is also needed for quantifying renal blood flow in ASL imaging (32) and optimizing the inversion time in non-contrast enhanced renal angiography studies (33). As tissue relaxation times are field-dependent and cannot be accurately predicted by theoretical calculation, *in vivo* studies must be performed to estimate these relaxation parameters. However, to date, no human studies have been performed to estimate renal relaxation times at 7T.

Measuring renal $T_1$ and $T_2$ is challenging due to respiratory motion. Although respiratory triggering can help reduce the resulting artifacts, an inconsistent respiratory rate and variations in end expiratory position between breaths can result in significant variations in kidney position confounding accurate image co-registration and subsequent relaxation time estimations (30). Therefore, single breath-hold imaging approaches are preferred. The two major imaging methods that have been predominantly used for renal tissue relaxation time estimations within a single breath-hold are true fast imaging with steady state precession (TrueFISP) (34) and single shot fast spin echo (ss-FSE) (35). Compared to TrueFISP, ss-FSE has improved tolerance to $B_0$ inhomogeneity. As field inhomogeneity increases with field strength, ss-FSE is arguably the preferred method to use for imaging readout at 7T. However, measuring renal $T_1$ and $T_2$ at 7T faces new challenges, including $B_1$+ inhomogeneity, reduced RF efficiency and specific absorption rate (SAR) limits which are more rapidly reached.

In this work, we describe a method based on an ss-FSE sequence that can measure renal longitudinal and transverse relaxation times at 7T within a single breath-hold. The $B_1$+ inhomogeneity and RF efficiency at 7T were managed by using subject dependent $B_1$+ shimming (8) and calibration. Using this technique, measurements of renal $T_1$ and $T_2$ values were acquired at both 3T and 7T in healthy normal volunteers. The reproducibility of these measurements at 7T was determined in repeated studies.

## MATERIALS AND METHODS

### Subjects

A total seven healthy volunteers (five males: 47 ± 17 years and two females: 34 ± 18 years, mean ± S.D.) provided written informed consent prior to being studied according to a local IRB approved protocol. Of the seven, five participated in all three studies: relaxometry studies at 3T and 7T, and repeat measurements at 7T. The repeat measurements at 7T were performed to determine reproducibility and involved two sessions about one week apart (6–8 days, median 7 days).

### MRI

3T MRI studies were performed on a Siemens TIM Trio MRI scanner (Malvern, Pennsylvania) with a 60 cm diameter horizontal magnet, a body coil for RF transmission, and a body surface array (two rows of 3 elements) anteriorly combined with the spine array (two rows of 3 elements) posteriorly for signal reception.

7T MRI studies were performed on a Siemens 7T whole body MRI scanner with 58 cm diameter horizontal bore, using a 16-channel transceiver TEM stripline array (10) driven by a series of sixteen 1 kW amplifiers (CPC, Pittsburgh, PA). The RF power deposition and reflection from each channel was monitored separately and continuously by using a power-monitoring system built in-house (17). The power limit set for each channel was based on simulation results and according to the IEC guidance (33).

### Imaging Sequences

A magnetization prepared single-shot fast spin echo (ss-FSE) imaging sequence was used for relaxometry measurements, as shown in Figure 1. $T_1$ mapping was performed using an inversion recovery preparation with variable inversion times (IR-prep ss-FSE). To achieve uniform inversion across and within an imaging slice, the inversion was performed using a slice-selective adiabatic hyperbolic secant RF pulse with an inversion slab that was twice the imaging slice thickness. At 3T, the inversion was achieved with a 15.36 ms hyperbolic secant pulse with 3 kHz bandwidth (36); at 7T an HS4 pulse with 20 ms duration and 1 kHz bandwidth was used (37). $T_2$ mapping was performed by inserting a Carr-Purcell-Meiboom-Gill (CPMG) style refocusing pulse train (38,39) after the excitation and prior to ss-FSE readout, and varying number of echoes in steps of two (CMPG-prep ss-FSE). The same echo spacing was used for both CPMG-prep and the ss-FSE readout.

With this approach, the $T_1$ and $T_2$ maps can each be acquired within a single breath-hold to minimize respiratory artifacts (35). At the beginning of both $T_1$ and $T_2$ acquisitions, a dummy scan was performed to establish spin steady state. The saturation recovery time (Ts) between successive measurements was kept constant to avoid variable $T_1$ weighting (Figure 1). To reduce short-term SAR at 7T, variable-rate selective excitation (VERSE) RF pulses (40) were used for excitation, and the hyperecho phase and amplitude modulation scheme was used for ss-FSE readout (41).

For 3T studies, a transverse imaging slice with a large field of view (FOV) was used to cover both kidneys. For 7T studies, a transverse imaging slice with a small FOV covering one side of the kidneys was used. Focusing on a signal kidney allowed greater $B_1$+ homogeneity with increased efficiency to minimize short-term SAR and to improve uniformity for the adiabatic inversion preparation.

### 3T Acquisition Parameters

For both $T_1$ and $T_2$ measurements, imaging parameters for the ss-FSE readout were: FOV = $360 \times 360$ mm$^2$, matrix size = $256 \times 256$, in-plane resolution = $1.4 \times 1.4$ mm$^2$, excitation/refocusing RF flip angles (FAs) = 90°/180°, slice thickness = 5 mm, anterior to posterior phase encoding direction, parallel imaging accelerator factor using GRAPPA = 2 with 24

separately acquired reference lines, partial Fourier = 4/8, total 7 measurements with the first one as a dummy scan. For $T_1$ measurements, the following parameters were used: TR/TE 3000/29 ms, bandwidth = 814 Hz/pixel and echo spacing = 4.12 ms, and inversion times = {100, 150, 300, 500, 800, 1200} ms; for $T_2$ measurements, TR/TE = 3000/35 ms, bandwidth = 476 Hz/pixel, echo spacing = 4.98 ms, and six different numbers of preparation echoes = {4, 8, 16, 24, 32, 40}. The total acquisition times were less than 23 s and 19 s for $T_1$ and $T_2$ measurements, respectively.

### 7T Acquisition Parameters

Imaging parameters for $T_1$ and $T_2$ measurements at 7 T were: TR = 3000–4000 ms, FOV = 192 × 192 $mm^2$, in-plane resolution = 1.5 × 1.5 $mm^2$, slice thickness = 5 mm, phase encoding direction = left-right or anterior-posterior with 50~80% oversampling, partial Fourier = 5/8, parallel imaging acceleration factor using GRAPPA = 4 with 24 separately acquired reference lines, and hyperecho flip angle = 90 degree. $T_1$ measurements used TE = 16 ms, 814 Hz/pixel bandwidth with 3.96 ms echo spacing. $T_2$ measurements used TE = 20 ms, 439 Hz/pixel bandwidth with 5.0 ms echo spacing. To further minimize short-term SAR for single breath-hold $T_1$ and $T_2$ imaging, the inversion times and the number of preparation echoes for six measurements were specifically arranged in the following order: {100, 1200, 150, 800, 300, 500} ms and {40, 4, 32, 8, 16, 24}, respectively. The maximal imaging acquisition times across all subjects were less than 29 s and 25 s for $T_1$ and $T_2$ measurements, respectively, with a 4 s repetition time.

### $B_0$ and $B_1$+ optimization

On both 3T and 7T, local $B_0$ optimization was accomplished by acquiring volumetric phase maps within a single breath-hold (42).

For 7T imaging, $B_1$+ optimization was performed in the selected kidney region by using phase-only $B_1$+ shimming, followed by a flip angle calibration over the same region. $B_1$+ shimming was performed by acquiring a small flip-angle calibration scan and optimizing $B_1$+ using a tradeoff between homogeneity and efficiency (33). $B_1$+ maps were subsequently generated using a 2D implementation of the Actual Flip-angle Imaging (AFI) technique (43) acquired in a single breath hold, with TR1/TR2/TE = 70/120/2.5 ms, FOV = 128 × 128 $mm^2$, matrix size = 64 × 64; in-plane resolution = 2 × 2 $mm^2$, slice thickness = 5 mm, and averages = 5. The 2D AFI implementation was corrected for the slice profile imperfection by using a scale factor of 1.5, as determined by a phantom calibration study. Flow compensation gradients were applied along both the slice and imaging readout directions to reduce flow artifacts during $B_1$+ shimming and $B_1$+ mapping acquisitions. An example of the $B_1$+ optimization ROI and associated flip angle map is shown in Figure 2.

### Image Processing and Data Analysis

Voxel-wise $T_1$ and $T_2$ mapping and region of interest (ROI)-based model fitting for $T_1$ and $T_2$ estimations were all performed in Matlab 7.1 (MathWorks, Natick, MA). The statistical analysis was performed in GraphPad Prism 5.0 (GraphPad Software Inc., La Jolla, CA). ROIs for renal cortex and medulla were conservatively defined to reduce partial volume effects. For $T_1$ measurements, ROIs were determined by using images acquired with an

inversion time (TI) near the nulling point for the medulla. For $T_2$ measurements, ROIs were defined on the $T_2$-weighted images that had the greatest contrast between the cortex and medulla. To further minimize partial volume effects and errors due to sporadic physiological noise, a trimmed mean was used for $T_1$ and $T_2$ estimations, excluding the 5% of voxels with the lowest values and the 5% with the highest values based on the histogram from each ROI (44). The number of voxels included in the renal cortex and medulla ROIs combined for a single kidney were 98 ± 30 and 118 ± 32 for 3T and 7T, respectively. For the estimation of background noise, 50 voxels were included.

### $T_1$ and $T_2$ Mapping and Estimation

$T_1$ and $T_2$ fitting were performed on a pixel-wise basis to produce relaxometric parametric maps. To reduce the bias for $T_1$ and $T_2$ estimations due to the relatively low SNR near the nulling point for the IR preparation and at long effective TEs, data were fit using models that incorporated image noise, as described previously (35). For images acquired at different inversion times, nonlinear least square model fitting was performed with the following equation:

$$S(TI)=\sqrt{[S_0(1-2\exp^{(-TI/T_1)}+\exp^{(-T_r/T_1)}]^2+C_{noise}^2}, \quad [1]$$

where S(TI) is the measured signal intensity at inversion time TI, $S_0$ the proton density image weighted by coil sensitivity and imaging gain, $T_1$ the tissue longitudinal relaxation time to be estimated, $T_r$ the recovery time after imaging saturation and $C_{noise}$ the estimated imaging noise. For images acquired with different TEs, the following equation was used:

$$S(TE)=\sqrt{[S_0\exp^{(-TE/T_2)}]^2+C_{noise}^2}, \quad [2]$$

where S(TE) is the measured signal intensity at each TE and $T_2$ is the tissue transverse relaxation time constant to be estimated.

### Statistical Analysis

Repeated measures two-way analysis of variance (ANOVA) was performed to determine statistical significance of differences in relaxometry values between renal tissue types and between field strengths. The Bonferroni post-test following ANOVA was applied for multiple comparisons between renal tissue types and field strengths. Statistical significance was defined as a P-value less than 0.05.

The reproducibility of $T_1$ and $T_2$ values measured at 7T was evaluated as percent difference between two sessions by using the following formula:

$$Difference(\%)=\frac{(S_1-S_2)}{(S_1+S_2)/2}\times 100, \quad [3]$$

where $S_1$ and $S_2$ are renal $T_1$ and $T_2$ measurements from the first and second sessions.

## RESULTS

$T_1$ and $T_2$ relaxometry measurements were successfully performed in all 7 subjects. Examples of 7T renal $T_1$ and $T_2$ mapping from a representative subject are presented in Figure 3. The estimated individual renal $T_1$ and $T_2$ values from 3T and the first session of 7T studies are presented in Figures 4a–4b, and group means and standard deviations of renal $T_1$ and $T_2$ values are listed in Table 1.

Repeated measures two-way ANOVA analysis showed no interaction effects between renal tissue type and field strength (P values = 0.83 and 0.73 for renal $T_1$ and $T_2$) but significant effects of these two factors on renal $T_1$ and $T_2$ values (P values <0.001 for both). Bonferroni post-test analysis showed significant differences between 3T and 7T for cortical and medullary $T_1$ (P values < 0.001) and $T_2$ (P values < 0.01 for renal cortex and < 0.05 for renal medulla), and between renal cortex and medulla for $T_1$ and $T_2$ measurements on 3T (P values < 0.001 for renal $T_1$ and < 0.01 for renal $T_2$) and 7T (P values < 0.001 for both renal $T_1$ and $T_2$).

Two-tailed paired t-tests showed insignificant differences in measured $T_1$ between the two 7T sessions (P values = 0.47 and = 0.94 for cortical and medullary $T_1$) and $T_2$ values (P values = 0.51 and = 0.15 cortical and medullary $T_2$). The 7T measurements of $T_1$ and $T_2$ were very reproducible with all group mean percent differences within 4% (Table 1 and Figure 4c–4d).

## DISCUSSION

This is the first study reporting normal renal $T_1$ and $T_2$ values at 7 T. While similar methods have been used in renal relaxometry studies at 3T, a number of adaptations were needed to overcome the challenges of ultra-high field MR, including increased $B_1$ and $B_0$ inhomogeneity, short-term SAR constraints, and limited RF peak power.

Having a uniform and efficient $B_1$+ shim was required in order to produce a uniform inversion for the $T_1$ measurements. With the $B_1$+ shimming and calibration techniques used here, the $B_1$+ variation over the kidney was small, with a typical coefficient of variation of ~8% (Figure 2). We verified that this was sufficient to provide uniform inversion with an adiabatic inversion pulse by observing that 1) scans acquired with the higher HS4 RF voltage did not significantly change renal $T_1$ measurements and 2) no significant differences were found between $T_1$ measurements in regions with high and low $B_1$+ amplitudes (data not shown). The $B_1$+ optimization was made substantially easier by focusing on a signal kidney with axial imaging slices.

Although using single breath-hold ss-FSE helps reduce respiration motion artifacts and is insensitive to $B_0$ inhomogeneity, short-term SAR is a limiting factor, especially as the ss-FSE readout is combined with the additional inversion and refocusing pulses used for $T_1/T_2$ encoding. A combination of multiple RF power-reducing strategies was used to minimize short-term SAR. First, the number of phase encoding lines was minimized by using partial Fourier imaging as well as a high parallel imaging acceleration factor of 4. Second, the hyperecho technique was used to reduce the flip angle of the readout pulses (41). Third, the

VERSE technique was used to reduce the peak power requirements for both excitation and refocusing pulses. Fourth, the $T_1$ measurement used interleaved long and short inversion times to better distribute the power deposition over time; likewise the $T_2$ measurement interleaved large and small numbers of preparation echoes. Finally, the parallel imaging reference scans were acquired only once per breath-hold rather than with each encoded acquisition. Since the required power varied between subjects, the shortest repetition time allowable under the short-term SAR limits was used in order the minimize breath-hold times.

To avoid partial volume effects on $T_1$ and $T_2$ estimations, conservative regions in the renal cortex and medulla were selected for data analysis. Furthermore, trimmed mean values within ROIs were used for final estimation to further remove possible errors due to partial volume effects and/or physiological noise.

Because of the challenges of performing relaxometry studies in the kidney, reported renal $T_1$ and $T_2$ in human are quite limited. Estimated 3T cortical and medullary $T_1$ values of the present study are comparable to those reported in the literature (1142 ± 154 ms and 1545 ± 142 ms for the cortex and medulla, respectively), but $T_2$ values are significantly higher than those previously reported (76 ± 7 ms and 81 ± 8 ms for the cortex and medulla, respectively) (35).

In the current study, $T_2$ contrast was achieved by using a Carr-Purcell-Meiboom-Gill (CPMG) style refocusing echo train rather than a single spin echo preparation (35). It is well known that the continuous application of refocusing RF pulses reduces signal loss due to molecular diffusion, field inhomogeneity and J coupling (45), resulting in longer $T_2$ estimates. $T_2$ values were indeed shorter at 3T when using a single spin echo preparation in both phantom and in vivo studies (data not shown). Estimates of renal $T_2$ values obtained by FSE imaging methods at 1.5T in another study (46) with reported mean $T_2$ values of 112 and 143 ms for the renal cortex and medulla, were also higher than the results using a single spin echo $T_2$ encoding (35). Since in practice, FSE imaging methods, such as segmented FSE and ss-FSE, are widely used for renal MRI, the protocol optimization for such imaging methods should be based on $T_2$ measurements that are estimated under similar conditions, which was the reason that the current strategy was used for estimating $T_2$.

It has been demonstrated that renal $T_1$ and $T_2$ imaging can be successfully performed at 7T in a single breath-hold, and that these $T_1$ and $T_2$ measurements were highly reproducible. However, due to short-term SAR constraints, mapping could only be achieved in a single kidney. To perform bilateral kidney relaxometry, multiple breath holds can be performed, but may be challenging for subjects in a clinical setting. Therefore, imaging methods with low RF power deposition suitable for $T_1$ and $T_2$ imaging are needed for UHF applications. It should also be noted, however, that even at lower field strengths, $T_1$ and $T_2$ mapping of the kidneys has been limited to a single slice acquisitions (29,30,46). The ability to obtain full coverage of the kidneys is still limited by respiratory motion and compounded by the challenge of accurate co-registration of images with varying contrast.

## CONCLUSION

In summary, renal longitudinal and transverse relaxation times can be reliably and reproducibly measured by using an ss-FSE measurement strategy within a single breath-hold at 7T.

## Acknowledgments

**Grant Sponsor:** National Institute of Health P41 EB015894 and S10 RR026783.

## Abbreviations used

| | |
|---|---|
| **ANOVA** | ANalysis Of VAriance |
| **ASL** | Arterial Spin Labeling |
| **AFI** | Actual Flip-angle Imaging |
| **CPMG** | Carr-Purcell-Meiboom-Gill |
| **FA** | Flip Angle |
| **FOV** | Field Of View |
| **GRAPPA** | GeneRalized Autocalibrating Partially Parallel Acquisitions |
| **MRI** | Magnetic Resonance Imaging |
| **ROI** | Region Of Interest |
| **ss-FSE** | single shot fast spin echo |
| **S.D** | Standard Deviation |
| **SAR** | Specific Absorption Rate |
| **SNR** | Signal Noise Ratio |
| **TE** | Echo Time |
| **TR** | Repetition Time |
| **TrueFISP** | TRue Fast Imaging with Steady Precession |
| **UHF** | Ultra High Field |
| **VERSE** | VariablE-Rate Selective Excitation |

## References

1. Ugurbil K. The road to functional imaging and ultrahigh fields. NeuroImage. 2012; 62(2):726–735. [PubMed: 22333670]
2. Kerchner GA. Ultra-high field 7T MRI: a new tool for studying Alzheimer's disease. Journal of Alzheimer's disease : JAD. 2011; 26 (Suppl 3):91–95.
3. Nakada T. Clinical application of high and ultra high-field MRI. Brain & development. 2007; 29(6): 325–335. [PubMed: 17113259]
4. Beisteiner R, Robinson S, Wurnig M, Hilbert M, Merksa K, Rath J, Hollinger I, Klinger N, Marosi C, Trattnig S, Geissler A. Clinical fMRI: evidence for a 7T benefit over 3T. NeuroImage. 2011; 57(3):1015–1021. [PubMed: 21620980]

5. von Morze C, Xu D, Purcell DD, Hess CP, Mukherjee P, Saloner D, Kelley DA, Vigneron DB. Intracranial time-of-flight MR angiography at 7T with comparison to 3T. Journal of magnetic resonance imaging : JMRI. 2007; 26(4):900–904. [PubMed: 17896360]
6. Vaughan JT, Garwood M, Collins CM, Liu W, DelaBarre L, Adriany G, Andersen P, Merkle H, Goebel R, Smith MB, Ugurbil K. 7T vs. 4T: RF power, homogeneity, and signal-to-noise comparison in head images. Magnetic resonance in medicine : official journal of the Society of Magnetic Resonance in Medicine / Society of Magnetic Resonance in Medicine. 2001; 46(1):24–30.
7. van den Bergen B, van den Berg CA, Klomp DW, Lagendijk JJ. SAR and power implications of different RF shimming strategies in the pelvis for 7T MRI. Journal of magnetic resonance imaging : JMRI. 2009; 30(1):194–202. [PubMed: 19557737]
8. Metzger GJ, Snyder C, Akgun C, Vaughan T, Ugurbil K, Van de Moortele PF. Local B1+ shimming for prostate imaging with transceiver arrays at 7T based on subject-dependent transmit phase measurements. Magnetic resonance in medicine : official journal of the Society of Magnetic Resonance in Medicine / Society of Magnetic Resonance in Medicine. 2008; 59(2):396–409.
9. Adriany G, Van de Moortele PF, Ritter J, Moeller S, Auerbach EJ, Akgun C, Snyder CJ, Vaughan T, Ugurbil K. A geometrically adjustable 16-channel transmit/receive transmission line array for improved RF efficiency and parallel imaging performance at 7 Tesla. Magnetic resonance in medicine : official journal of the Society of Magnetic Resonance in Medicine / Society of Magnetic Resonance in Medicine. 2008; 59(3):590–597.
10. Snyder CJ, Delabarre L, Moeller S, Tian J, Akgun C, Van de Moortele PF, Bolan PJ, Ugurbil K, Vaughan JT, Metzger GJ. Comparison between eight- and sixteen-channel TEM transceive arrays for body imaging at 7 T. Magnetic resonance in medicine : official journal of the Society of Magnetic Resonance in Medicine / Society of Magnetic Resonance in Medicine. 2012; 67(4):954–964.
11. Thomas BP, Welch EB, Niederhauser BD, Whetsell WO Jr, Anderson AW, Gore JC, Avison MJ, Creasy JL. High-resolution 7T MRI of the human hippocampus in vivo. Journal of magnetic resonance imaging : JMRI. 2008; 28(5):1266–1272. [PubMed: 18972336]
12. Grams AE, Kraff O, Umutlu L, Maderwald S, Dammann P, Ladd ME, Forsting M, Gizewski ER. MRI of the lumbar spine at 7 Tesla in healthy volunteers and a patient with congenital malformations. Skeletal radiology. 2012; 41(5):509–514. [PubMed: 21604210]
13. Kollia K, Maderwald S, Putzki N, Schlamann M, Theysohn JM, Kraff O, Ladd ME, Forsting M, Wanke I. First clinical study on ultra-high-field MR imaging in patients with multiple sclerosis: comparison of 1. 5T and 7T. AJNR American journal of neuroradiology. 2009; 30(4):699–702. [PubMed: 19147714]
14. Tallantyre EC, Morgan PS, Dixon JE, Al-Radaideh A, Brookes MJ, Morris PG, Evangelou N. 3 Tesla and 7 Tesla MRI of multiple sclerosis cortical lesions. Journal of magnetic resonance imaging : JMRI. 2010; 32(4):971–977. [PubMed: 20882628]
15. Vaughan JT, Snyder CJ, DelaBarre LJ, Bolan PJ, Tian J, Bolinger L, Adriany G, Andersen P, Strupp J, Ugurbil K. Whole-body imaging at 7T: preliminary results. Magnetic resonance in medicine : official journal of the Society of Magnetic Resonance in Medicine / Society of Magnetic Resonance in Medicine. 2009; 61(1):244–248.
16. Suttie JJ, Delabarre L, Pitcher A, van de Moortele PF, Dass S, Snyder CJ, Francis JM, Metzger GJ, Weale P, Ugurbil K, Neubauer S, Robson M, Vaughan T. 7 Tesla (T) human cardiovascular magnetic resonance imaging using FLASH and SSFP to assess cardiac function: validation against 1. 5 T and 3 T. NMR in biomedicine. 2012; 25(1):27–34. [PubMed: 21774009]
17. Metzger GJ, van de Moortele PF, Akgun C, Snyder CJ, Moeller S, Strupp J, Andersen P, Shrivastava D, Vaughan T, Ugurbil K, Adriany G. Performance of external and internal coil configurations for prostate investigations at 7 T. Magnetic resonance in medicine : official journal of the Society of Magnetic Resonance in Medicine / Society of Magnetic Resonance in Medicine. 2010; 64(6):1625–1639.
18. van de Bank BL, Voogt IJ, Italiaander M, Stehouwer BL, Boer VO, Luijten PR, Klomp DW. Ultra high spatial and temporal resolution breast imaging at 7T. NMR in biomedicine. 2012
19. Umutlu L, Maderwald S, Kinner S, Kraff O, Bitz AK, Orzada S, Johst S, Wrede K, Forsting M, Ladd ME, Lauenstein TC, Quick HH. First-pass contrast-enhanced renal MRA at 7 Tesla: initial results. European radiology. 2012

20. Kinner S, Dechene A, Paul A, Umutlu L, Ladd SC, de Dechene EM, Zopf T, Gerken G, Lauenstein TC. Detection of biliary stenoses in patients after liver transplantation: is there a different diagnostic accuracy of MRCP depending on the type of biliary anastomosis? European journal of radiology. 2011; 80(2):e20–28. [PubMed: 20580506]
21. Umutlu L, Bitz AK, Maderwald S, Orzada S, Kinner S, Kraff O, Brote I, Ladd SC, Schroeder T, Forsting M, Antoch G, Ladd ME, Quick HH, Lauenstein TC. Contrast-enhanced ultra-high-field liver MRI: A feasibility trial. European journal of radiology. 2011
22. Korteweg MA, Veldhuis WB, Visser F, Luijten PR, Mali WP, van Diest PJ, van den Bosch MA, Klomp DJ. Feasibility of 7 Tesla breast magnetic resonance imaging determination of intrinsic sensitivity and high-resolution magnetic resonance imaging, diffusion-weighted imaging, and (1)H-magnetic resonance spectroscopy of breast cancer patients receiving neoadjuvant therapy. Investigative radiology. 2011; 46(6):370–376. [PubMed: 21317792]
23. XL; P-F; VdM; KU; GM. Dynamically Applied Multiple B1+ Shimming Scheme for Arterial Spin Labeling of the Prostate at 7T. Proceedings of the 19th Annual Meeting of ISMRM; Montréal, Québec, Canada. 2011; 2011. p. Abstract 593
24. Li, X.; Ugurbil, K.; Metzger, GJ. Theoretical Evaluation of Ultra High Field Benefits to Non-contrast Enhanced Renal Perfusion Imaging Using FAIR-EPI. Proceedings of the 201h Annual Meeting of ISMRM; Salt Lake City, USA. 2013; p. Abstract 1540
25. Li, X.; Snyder, C.; Van de Moortele, P-F.; Ugurbil, K.; Metzger, GJ. Non-Contrast Enhanced Human Renal Perfusion Imaging Using Arterial Spin Labeling at 7 T: Initial Experience. Proceedings of the 20th Annual Meeting of ISMRM; Melbourne, Australia. 2012; p. Abstract 1310
26. Li, X.; Snyder, C.; Van de Moortele, P-F.; Ugurbil, K.; Metzger, GJ. Feasibility of Single Breath-hold Renal Perfusion Imaging at 7T. Proceedings of the 201h Annual Meeting of ISMRM; Salt Lake City, USA. 2013; p. Abstract 30
27. Nikken JJ, Krestin GP. MRI of the kidney-state of the art. European radiology. 2007; 17(11):2780–2793. [PubMed: 17646992]
28. Terrier F, Hricak H, Justich E, Dooms GC, Grodd W. The diagnostic value of renal cortex-to-medulla contrast on magnetic resonance images. European journal of radiology. 1986; 6(2):121–126. [PubMed: 3522232]
29. Lee VS, Kaur M, Bokacheva L, Chen Q, Rusinek H, Thakur R, Moses D, Nazzaro C, Kramer EL. What causes diminished corticomedullary differentiation in renal insufficiency? Journal of magnetic resonance imaging : JMRI. 2007; 25(4):790–795. [PubMed: 17335025]
30. Huang Y, Sadowski EA, Artz NS, Seo S, Djamali A, Grist TM, Fain SB. Measurement and comparison of T1 relaxation times in native and transplanted kidney cortex and medulla. Journal of magnetic resonance imaging : JMRI. 2011; 33(5):1241–1247. [PubMed: 21509885]
31. Semelka RC, Corrigan K, Ascher SM, Brown JJ, Colindres RE. Renal corticomedullary differentiation: observation in patients with differing serum creatinine levels. Radiology. 1994; 190(1):149–152. [PubMed: 8259395]
32. Martirosian P, Klose U, Mader I, Schick F. FAIR true-FISP perfusion imaging of the kidneys. Magnetic resonance in medicine : official journal of the Society of Magnetic Resonance in Medicine / Society of Magnetic Resonance in Medicine. 2004; 51(2):353–361.
33. Metzger GJ, Auerbach EJ, Akgun C, Simonson J, Bi X, Ugurbil K, van de Moortele PF. Dynamically applied B1+ shimming solutions for non-contrast enhanced renal angiography at 7. 0 Tesla. Magnetic resonance in medicine : official journal of the Society of Magnetic Resonance in Medicine / Society of Magnetic Resonance in Medicine. 2013; 69(1):114–126.
34. Bokacheva L, Huang AJ, Chen Q, Oesingmann N, Storey P, Rusinek H, Lee VS. Single breath-hold T1 measurement using low flip angle TrueFISP. Magnetic resonance in medicine : official journal of the Society of Magnetic Resonance in Medicine / Society of Magnetic Resonance in Medicine. 2006; 55(5):1186–1190.
35. de Bazelaire CM, Duhamel GD, Rofsky NM, Alsop DC. MR imaging relaxation times of abdominal and pelvic tissues measured in vivo at 3. 0 T: preliminary results. Radiology. 2004; 230(3):652–659. [PubMed: 14990831]

36. Li X, Sarkar SN, Purdy DE, Haley RW, Briggs RW. Improved quantification of brain perfusion using FAIR with active suppression of superior tagging (FAIR ASST). Journal of magnetic resonance imaging : JMRI. 2011; 34(5):1037–1044. [PubMed: 22002755]
37. Garwood M, DelaBarre L. The return of the frequency sweep: designing adiabatic pulses for contemporary NMR. Journal of magnetic resonance. 2001; 153(2):155–177. [PubMed: 11740891]
38. Carr HY, Purcell EM. Effects of Diffusion on Free Precession in Nuclear Magnetic Resonance Experiments. Physical Review. 1954; 94(3):630–638.
39. Meiboomm S, GD. Modified Spin-Echo Method for Measuring Nuclear Relaxation Times. Review of Scientific Instruments. 1958; 29(8):688–691.
40. Hargreaves BA, Cunningham CH, Nishimura DG, Conolly SM. Variable-rate selective excitation for rapid MRI sequences. Magnetic resonance in medicine : official journal of the Society of Magnetic Resonance in Medicine / Society of Magnetic Resonance in Medicine. 2004; 52(3):590–597.
41. Hennig J, Scheffler K. Hyperechoes. Magnetic resonance in medicine : official journal of the Society of Magnetic Resonance in Medicine / Society of Magnetic Resonance in Medicine. 2001; 46(1):6–12.
42. Shah, S.; Kellman, P.; Greiser, A.; Weale, PJ.; Zuehlsdorff, S.; Jerecic, aR. Rapid Fieldmap Estimation for Cardiac Shimming. Proceedings of the 17th Annual Meeting of ISMRM; Honolulu, Hawai'i, USA. 2009; p. Abstract 566
43. Yarnykh VL. Actual flip-angle imaging in the pulsed steady state: a method for rapid three-dimensional mapping of the transmitted radiofrequency field. Magnetic resonance in medicine : official journal of the Society of Magnetic Resonance in Medicine / Society of Magnetic Resonance in Medicine. 2007; 57(1):192–200.
44. Li X, Sarkar SN, Purdy DE, Spence JS, Haley RW, Briggs RW. Anteroposterior perfusion heterogeneity in human hippocampus measured by arterial spin labeling MRI. NMR in biomedicine. 2013; 26(6):613–621. [PubMed: 23420779]
45. Carr HY, Purcell EM. Effects of diffusion on free precession in nuclear magnetic resonace experiments. Physical Review. 1954; 94:630–638.
46. Zhang, JL.; Storey, P.; Rusineck, H.; Chandarana, H.; Bhatta, R.; Stoffel, D.; Sigmund, EE.; Chen, Q.; Lee, VS. Reproducibility of R2* and R2 measurements in human kidneys. Proceedings of the 19th Annual Meeting of ISMRM; Montréal, Québec, Canada. 2011; p. Abstract 2954

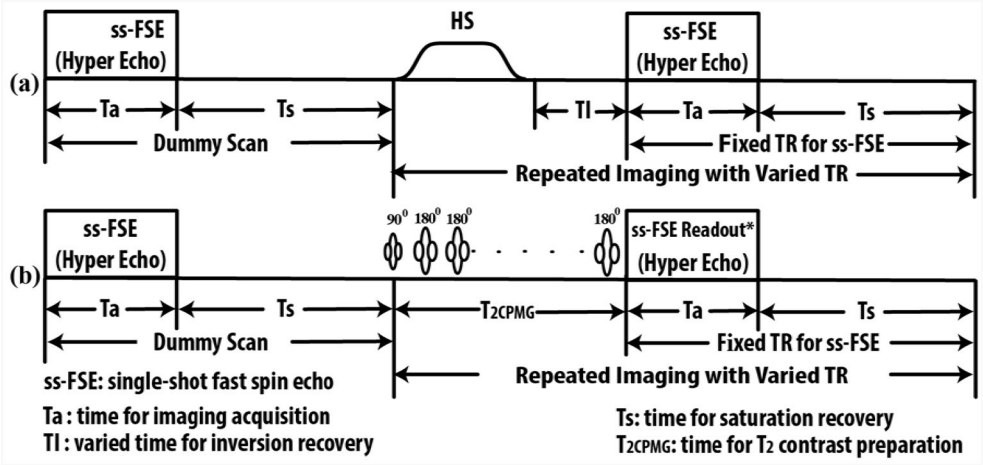


**Figure 1.**

$T_1$ and $T_2$ mapping sequence diagrams: (a) Sequence diagram for $T_1$ mapping using varied inversion times after an initial dummy scan. Inversion was accomplished by a hyperbolic secant (HS) RF pulse. (b) Sequence diagram for $T_2$ mapping using a Carr-Purcell-Meiboom-Gill style refocusing echo train ($T_{2CPMG}$) with varying numbers of refocusing echoes. To minimize the short-term specific absorption rate (SAR) at 7T, the ss-FSE readout employed the use of hyperechoes. Note: *ss-FSE readout refers to the data sampling for refocused echoes excluding the RF excitation.

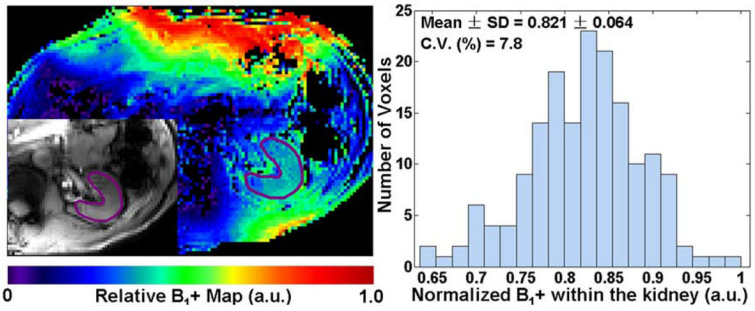


**Figure 2.**

Relative $B_1$+ map and histogram of normalized B1+ obtained from within the kidney for a representative subject. The ROI for evaluating the $B_1$+ distribution is illustrated with an anatomic image (inset on the left image). C.V. represents coefficient of variance, calculated as the ratio of standard deviation over mean.

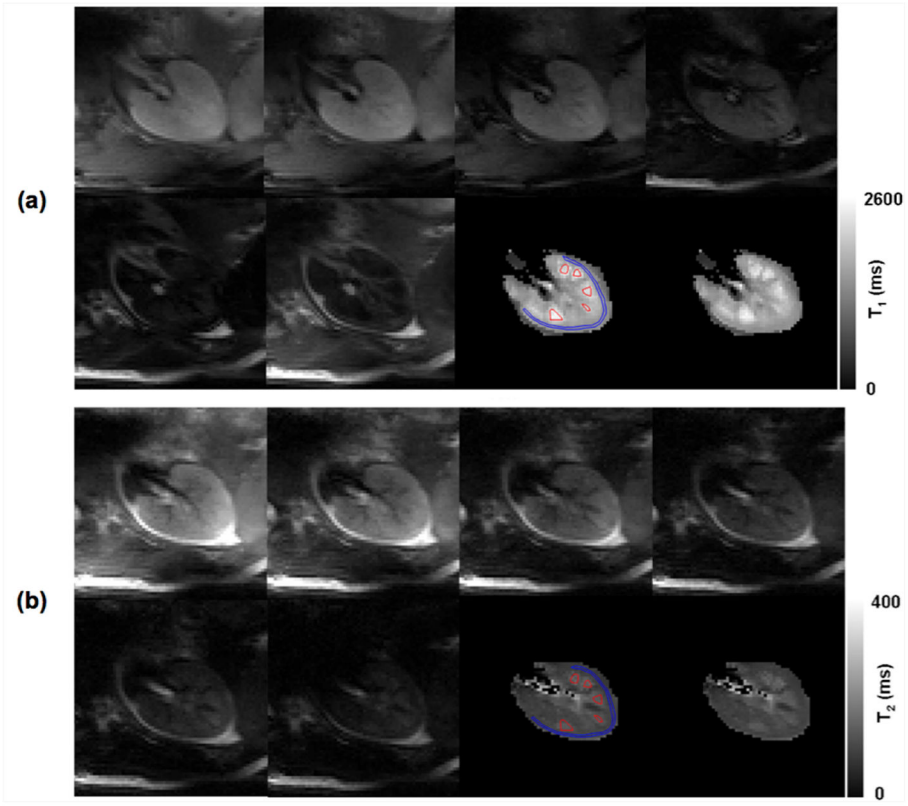


**Figure 3.**

7T $T_1$ and $T_2$ imaging results from one typical subject: (a) ss-FSE images were acquired by using six inversion times 100, 150 300, 500, 800 and 1200 ms; (b) ss-FSE images were acquired by using six different effective echo times: 20, 40, 80, 120, 160, and 200 ms. The conservatively defined ROIs (blue for the cortex and red for the medulla) used for the estimation of renal $T_1$ and $T_2$ are overlaid on the $T_1$ and $T_2$ maps generated from pixel-wise fitting.

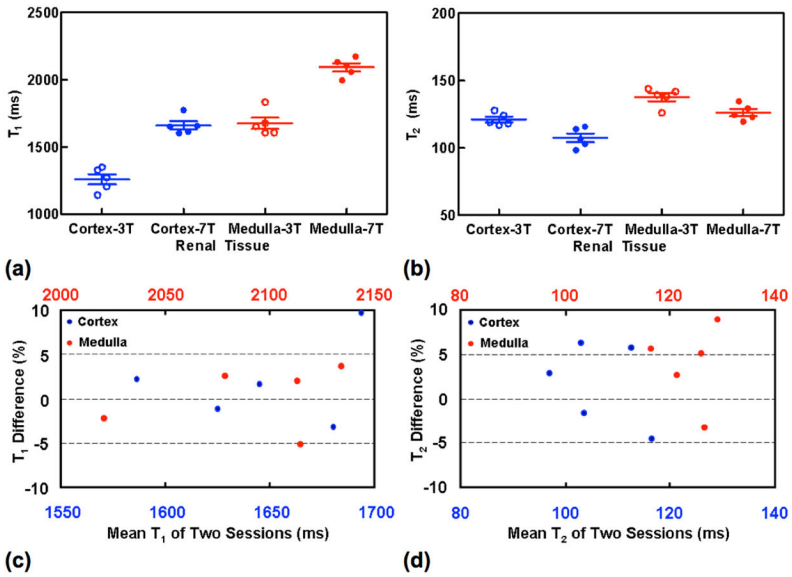


**Figure 4.**

Renal $T_1$ and $T_2$ measurements at 3T and 7T (a–b) and the reproducibility of renal $T_1$ and $T_2$ measurements at 7T (c–d) from five subjects. The presented renal $T_1$ and $T_2$ measurements at 7T in (a–b) are from the first session studies.

**Table 1**

Renal $T_1$ and $T_2$ measurements at 3T and 7T (mean ± S.D. ms) and percentage differences between two sessions at 7T from five subjects.

| | | Cortex | | Medulla | |
|---|---|---|---|---|---|
| | | $T_1$ | $T_2$ | $T_1$ | $T_2$ |
| **3T** | | **1261 ± 86** | **121 ± 5** | **1676 ± 94** | **138 ± 7** |
| **7T** | **1st Session** | 1661 ± 68 | 108 ± 7 | 2094 ± 67 | 126 ± 6 |
| | **2nd Session** | 1632 ± 49 | 106 ± 9 | 2091 ± 51 | 122 ± 6 |
| | **Difference (%)** | 1.8 ± 4.9 | 1.7 ± 4.7 | 0.1 ± 3.7 | 3.7 ± 4.5 |